Clim. Past Discuss., 10, 2767–2804, 2014
www.clim-past-discuss.net/10/2767/2014/
doi:10.5194/cpd-10-2767-2014

Climate of the Past Discussions
Open Access

Effect of the Ordovician paleogeography on the (in)stability of the climate

A. Pohl[1], Y. Donnadieu[1], G. Le Hir[2], J.-F. Buoncristiani[3], and E. Vennin[3]

[1]LSCE – Laboratoire des Sciences du Climat et de l'Environnement UMR8212 – CNRS-CEA-UVSQ, CEA Saclay, Orme des Merisiers, 91191 Gif-sur-Yvette Cedex, France
[2]IPGP – Institut de Physique du Globe de Paris, Université Paris7-Denis Diderot, 1 rue Jussieu, 75005 Paris, France
[3]Laboratoire Biogéosciences UMR/CNRS 6282, Université de Bourgogne, 6 Bd Gabriel, 21000 Dijon, France

Received: 23 May 2014 – Accepted: 9 June 2014 – Published: 2 July 2014

Correspondence to: A. Pohl (alexandre.pohl@lsce.ipsl.fr)

Published by Copernicus Publications on behalf of the European Geosciences Union.

Abstract

The Ordovician is a particular Period during Earth History highlighted by abundant evidence for continental-size polar ice-sheets. Modelling studies published so far require a sharp CO_2 drawdown to initiate this glaciation. They mostly used non-dynamic slab mixed-layer ocean models. Here, we use a general circulation model with coupled components for ocean, atmosphere and sea ice to examine the response of Ordovician climate to changes in CO_2 and paleogeography. We conduct experiments for a wide range of CO_2 (from 16 to 2 times the preindustrial atmospheric CO_2 level (PAL)) and for two continental configurations (at 470 Ma and at 450 Ma) mimicking the Middle and the Late Ordovician conditions. We find that the temperature–CO_2 relationship is highly non-linear when ocean dynamics is taken into account. Two climatic modes are simulated as radiative forcing decreases. For high CO_2 concentrations ($\geq$ 12 PAL at 470 Ma and $\geq$ 8 PAL at 450 Ma), a relative hot climate with no sea ice characterises the warm mode. When CO_2 is decreased to 8 PAL and 6 PAL at 470 and 450 Ma, a tipping-point is crossed and climate abruptly enters a runaway icehouse leading to a cold mode marked by the extension of the sea ice cover down to the mid-latitudes. At 450 Ma, the transition from the warm to the cold mode is reached for a decrease in atmospheric CO_2 from 8 to 6 PAL and induces a $\sim 9\,^{\circ}C$ global cooling. We show that the tipping-point is due to the existence of a quasi-oceanic Northern Hemisphere, which in turn induces a minimum in oceanic heat transport located around 40° N. The peculiar shape of the oceanic heat transport in the Northern Hemisphere explains the potential existence of the warm and of the cold climatic modes. This major climatic instability potentially brings a new explanation to the sudden Late Ordovician Hirnantian glacial pulse that does not require any large CO_2 drawdown.

CPD
10, 2767–2804, 2014

1 Introduction

The Ordovician Period reflects fundamental changes in the living organisms of our planet. Following the Cambrian Explosion, the Early Ordovician is characterized by a major radiation in marine life and critical changes in paleoecology during the Great Ordovician Biodiversification Event (GOBE) through the rise of the Paleozoic Evolutionary Fauna (Servais et al., 2010). This time of marine diversification is yet interrupted by the second of the five biggest extinctions of the Phanerozoic Eon in terms of the percentage of genera and families lost (Sheehan, 2001). Trotter et al. (2008) proposed a critical role of the oceanic thermal state during the GOBE, showing that the long-term cooling from a very warm ocean to present-day-like temperatures during the Early to Middle Ordovician may have led to optimal conditions for widespread taxonomic radiations and the appearance of complex communities. Cooler conditions in the Late Ordovician are generally associated with the onset of large ice-sheets over the Southern Gondwana (e.g., Ghienne et al., 2007). The growth and the drawdown of these ice-sheets are concomittent with the two pulses of the global extinction (Sheehan, 2001). Thus, a very close binding relationship may have existed between global climate and animal evolution during the Ordovician.

Atmospheric CO_2 concentration largely constrained climate evolution over Earth History (Berner, 2006). The Ordovician glaciation remains yet unusual since it occurred under high CO_2 values. Climate proxies (Yapp and Poths, 1992) and continental weathering models (Berner, 2006; Nardin et al., 2011) indicate that the Ordovician CO_2 atmospheric partial pressure (pCO_2) was equal to some 8–20 times its preindustrial atmospheric level (1 PAL = 280 ppm). The Faint Young Sun paradox (Gough, 1981) reduces somewhat this apparent discrepancy between high CO_2 levels and glacial inception by suggesting that the solar constant was lower in the past. Nevertheless, it seems not sufficient and the best hypotheses to trigger the Ordovician glaciation consider today a Late Ordovician drop in CO_2 (Brenchley et al., 1994; Kump et al., 1999; Villas et al., 2002; Lenton et al., 2012). A glacial threshold of 14 PAL to 8 PAL has been found with

CPD
10, 2767–2804, 2014

various models, from a conceptual EBM (Crowley and Baum, 1991) to a more complex GCM coupled to an ice-sheet model (Herrmann et al., 2003). Various data suggest that the lower CO_2 levels are probably the best estimates (Vandenbroucke et al., 2010; Pancost et al., 2013).

While the role of the pCO_2 has been fully investigated to explain the Ordovician glacial onset, much less has been done about the effect of ocean dynamics. Most of the modelling studies used atmospheric general circulation models (GCM) with slab mixed-layer oceans (Crowley et al., 1993; Crowley and Baum, 1995; Gibbs et al., 1997; Herrmann et al., 2003, 2004b). In these models, there are no currents and the poleward oceanic heat transport (OHT) is prescribed through a diffusion coefficient. Ocean dynamics is thus totally absent. Herrmann et al. (2004b) gave a precursory approach of this question by alterating the diffusion coefficient in the slab model GENESIS. They found that the paleogeographic evolution and a drop in CO_2 were only preconditioning factors that were not sufficient to trigger continental glaciation during the Hirnantian. Additional changes, such as a sea level drop or a lowered OHT, were necessary to cause glaciation within a reasonable CO_2 interval (8–18 PAL). These results suggest that ocean played a fundamental role in the Late Ordovician. But, as Herrmann et al. (2004a) noticed later, the non-dynamical ocean precluded any further investigation. Only two studies have so far investigated the role of ocean dynamics in the Late Ordovician climate changes. Poussart et al. (1999) coupled an energy/moisture balance model to an oceanic GCM and to a sea ice model. They demonstrated that the Ordovician geographic configuration may have led to critical changes in the OHT with an up to 42 % increase in the Southern OHT compared to present-day and a highly asymmetric OHT relative to the Equator. These results point out a major limitation inherent to the slab models that are unable to explicitely resolve the OHT, which value and pattern are often prescribed based on present-day estimates. Poussart et al. (1999) also demonstrated a strong sensitivity of the oceanic overturning circulation to changes in the ice-snow albedo parameters, highlighting a strong coupling between atmospheric and oceanic components in the Ordovician climate. Herrmann et al. (2004a) forced an

CPD
10, 2767–2804, 2014

oceanic GCM with the GENESIS outputs from Herrmann et al. (2004b). They compared the results obtained for two Late Ordovician paleogeographical configurations. They noticed a significant impact of paleogeography on the oceanic overturning circulation and thus on the OHT. They moreover demonstrated a non-linear response of the OHT to the atmospheric forcing. Their uncoupled modelling procedure however did not allow for any feedback of ocean on global climate.

Here, we propose to extend previous studies by exploring the effects of changed radiative forcing due to CO_2 decrease on the Ordovician climate with the fully coupled ocean–atmosphere-sea ice GCM FOAM (Jacob, 1997) for two time periods, the Middle Ordovician (Dapingian, 470 Ma) and the Late Ordovician (Katian, 450 Ma). The climate model and the experimental setup are briefly described in Sect. 2. The modelling results are presented in Sect. 3. The main results are discussed in Sect. 4 and a conclusion is given in Sect. 5.

2 Model description and experimental setup

2.1 The coupled climate model FOAM

We used the Fast Ocean–Atmosphere Model (FOAM) version 1.5, a 3-D GCM with coupled components for ocean, atmosphere and sea ice (Jacob, 1997). The atmospheric module is a parallelized version of NCAR's Community Climate Model 2 (CCM2) with the upgraded radiative and hydrologic physics from CCM3 version 3.2 (Kiehl et al., 1998). It was run at a R15 spectral resolution (4.5° x 7.5°) with 18 vertical levels. The ocean module, the Ocean Model version 3 (OM3), is a 24-level z-coordinate ocean GCM providing a 1.4° x 2.8° resolution. The sea ice module uses the thermodynamic component of the CSM1.4 sea ice model, which is based on the Semtner 3-layer thermodynamic snow/ice model (Semtner, 1976). The coupled model, FOAM, is well designed for paleoclimate studies. It has no flux corrections and its quick turnaround time allows for long millennium-scale integrations. FOAM has been widely used in paleocli-

CPD
10, 2767–2804, 2014

mate studies (Poulsen and Jacob, 2004; Donnadieu et al., 2009; Zhang et al., 2010; Dera and Donnadieu, 2012; Lefebvre et al., 2012) including for the Ordovician (Nardin et al., 2011).

2.2 Experimental setup

Spjeldnaes (1962), working on floro-faunal data, was the first to postulate a glaciation during the Ordovician. Since then, numerous studies widely documented the Ordovician glacial sedimentary record in North Africa (e.g., Beuf et al., 1971; Denis et al., 2007; Ghienne et al., 2007), South Africa (e.g., Young et al., 2004) and South America (e.g., Díaz-Martínez and Grahn, 2007). Dating these deposits remains highly difficult (e.g., Díaz-Martínez and Grahn, 2007) and geochemical methods bring conflicting results (see for example Trotter et al., 2008 and Finnegan et al., 2011). As a consequence, the duration of the glaciation is still not well constrained. Two models are still debated: a short-lived (< 2 Myr) glaciation limited to the Late Ordovician Hirnantian (445–443 Ma) (Brenchley et al., 1994, 2003; Sutcliffe et al., 2000), or a long-lived glaciation (> 20 Myr) that extended from the Late Ordovician Katian to the Silurian Wenlock, with the Hirnantian only representing the glacial maximum (Saltzman and Young, 2005; Loi et al., 2010; Finnegan et al., 2011) (Fig. 1). Some authors even propose a Darriwilian Ice Age based on eustatic cyclicities (Turner et al., 2012).

In this study, simulations were carried out for 2 paleogeographical configurations reconstructed by Blakey (2007), one for 470 Ma (Middle Ordovician Dapingian) and one for 450 Ma (Late Ordovician Katian) (Fig. 1). These two reconstructions have been chosen to be respectively representative of: (i) the pre-glacial interval; (ii) the undisputable Late Ordovician glacial interval. The 450 Ma reconstruction is considered here as a good estimate for the Late Ordovician Hirnantian (445 Ma). The paleogeographical changes are limited at that timescale and they are assumed to not critically impact global climate. Since previous studies have revealed the major role played by the topography to initiate glacial conditions during the Ordovician (Crowley and Baum, 1995), we defined five realistic topographic classes (Fig. 1). The ocean model bathymetry is a flat-

CPD
10, 2767–2804, 2014

bottom case. As Ordovician vegetation was limited to non-vascular plants (Steemans et al., 2009; Rubinstein et al., 2010) – the coverage of these can hardly be estimated – we imposed a bare soil (rocky desert) at every land grid point, probably the most representative land type at this time. The solar luminosity was set 3.5 % below present according to the Faint Young Sun paradox (Gough, 1981), and we used a cold summer orbit (CSO) like an orbital configuration. The CSO is defined with an obliquity of 22.5°, an eccentricity of 0.05 and a longitude of perihelion of 270°. Because most explanatory hypotheses require a major pCO_2 fall to initiate glacial conditions in the Middle–Late Ordovician (Brenchley et al., 1994; Kump et al., 1999; Villas et al., 2002; Lenton et al., 2012), we finally used five pCO_2 values representative for presumed Ordovician conditions: 4, 6, 8, 12 and 16 PAL. A lower value, 2 PAL, was also tested in order to better understand the climatic behaviour although this pCO_2 clearly stands beyond the lower bound of the pCO_2 range defined for the Ordovician Period. For each simulation, the model was run until deep ocean equilibrium was reached, which means 2000 years of integration except for the 450 Ma experiment with the pCO_2 set to 6 PAL that required 1000 years more.

3 Climate simulation results

3.1 Sensitivity to an atmospheric CO_2 decrease

Figure 2 presents the relationship between the global mean surface air temperature (SAT) and the pCO_2 for all the simulations discussed in this paper. For comparison with the previous studies done with slab oceans (Crowley et al., 1993; Crowley and Baum, 1995; Gibbs et al., 1997; Herrmann et al., 2003, 2004b), we first ran FOAM with a 50 m deep mixed-layer slab ocean (black dashed lines in Fig. 2). All boundary conditions were kept the same as for the runs with the ocean–atmosphere GCM (see Sect. 2.2) and we followed the usual conventions by setting the diffusion coefficient so that total OHT reaches its present value. As expected from previous studies, the Or-

CPD
10, 2767–2804, 2014

dovician climate system is well sensitive to a pCO_2 decrease and the temperature-CO_2 relationship is linear in a log-axis graph (Fig. 2a). The model sensitivity, 3 °C per halving of CO_2, lies very close to the value 2.5 °C obtained by Herrmann et al. (2003). It is however noteworthy that, for an identical atmospheric forcing value, climate is systematically warmer compared to GENESIS (Gibbs et al., 1997; Herrmann et al., 2004b). An immediate explanation lies in the prescribed solar constant. We chose a solar constant 3.5 % weaker than today following the parametric law from Gough (1981). Previous studies mostly used a 4.5 % depressed insolation compared to present-day (Crowley and Baum, 1995; Gibbs et al., 1997; Herrmann et al., 2003, 2004b), following the constant rate of decrease of 1 % every hundred million years proposed by Crowley and Baum (1992). Both values are within the range −3.5 to −5 % defined by Endal and Sofia (1981), but our weaker decrease of the solar constant logically results in higher temperatures. We must notice that modelled absolute temperatures are also sensitive to ice albedo and cloud parameterizations and are thus highly model-dependent (see for example Braconnot et al., 2012). Proposing absolute climate estimates for the Ordovician remains highly challenging and lies far beyond the main purpose of our study. Aside that absolute temperature offset, FOAM produces a trend similar to results previously published when it is used as a slab.

Using the same (450 Ma) paleogeographical configuration, FOAM experiments with ocean dynamics lead to a much different climatic response to the CO_2 forcing. The temperature-CO_2 relationship is non-linear (Fig. 2a). Two climatic modes are simulated as forcing parameters slowly change.

- For high CO_2 concentrations (≥ 8 PAL), the warm mode is marked by a hot climate (Figs. 2a and 3) and no sea ice in the Northern Hemisphere (NH) (Figs. 2b and 3). The model sensitivity is similar to the one obtained with the slab (3 °C per halving of CO_2) and lies within the range 2.1–4.7 °C defined with various up-to-date GCM for present-day simulations (IPCC, 2013). The temperature decrease associated to a CO_2 drop is almost evenly distributed at all latitudes (Fig. 4).

CPD
10, 2767–2804, 2014

– When atmospheric forcing is decreased from 8 PAL to 4 PAL, the annual global mean SAT falls by 8.65 °C from 8 PAL to 6 PAL, and by 7.6 °C from 6 PAL to 4 PAL. The Ordovician climate abruptly enters a cool climatic mode characterised by a fast extension of the sea ice cover (Figs. 2, 3 and 5). A tipping-point is reached, a slight pCO_2 drop leading to a sharp cooling. The temperature decrease associated to a halving of CO_2 (from 8 PAL to 4 PAL), −16 °C, lies far beyond the IPCC (2013) upper bound. The SAT drop is unevenly distributed against the latitudes. The minimum mean annual cooling is observed in the tropics (up to −5 °C from 8 PAL to 6 PAL) whereas the maximum cooling (up to −27 °C from 8 PAL to 6 PAL) occurs in both hemispheres at polar latitudes (Fig. 4). The amplification of the thermal response at high latitudes is due to the sea ice albedo positive feedback. The hemispheric sea ice cover (Table 1, Fig. 5b and c) suggests in particular a strong relationship between the NH sea ice extension and the global climate state. No ice is present in the NH within the warm mode (Fig. 3), and it is the expansion of the sea ice from the North Pole that marks the shift to the cold climatic mode.

– From 4 PAL to 2 PAL, the Earth's climate is still in cold mode but the SAT drop tends to slow down. Another threshold is crossed and the model sensitivity decreases back to a level characteristic of glacial climate (~ 5 °C per CO_2 halving, see Berner and Kothavala, 2001). The climate change does not differ so much from the cooling occurring within the warm climatic mode between 16 PAL and 8 PAL for a corresponding halving of CO_2, though glacial conditions still provide a higher global sensitivity (Kothavala et al., 1999) and an enhanced polar cooling. Sea ice continues to grow almost with the same intensity in the Southern Hemisphere (SH) but its spread is very limited in the NH (Table 1), where the sea ice edge stabilizes near 40° N (Fig. 5a).

The simulations were replicated for the 470 Ma continental configuration. Results are summarized in Table 1. A similar evolution is observed (Fig. 2), with two phases of

CPD
10, 2767–2804, 2014

stable climate separated by a major climatic instability (within the interval 12 PAL–6 PAL). The tipping-point showing the shift from the warm to the cold climatic mode is reached this time between 12 PAL and 8 PAL and is still associated to a sudden extension of the sea ice in the NH. Three main conclusions follow from theses results: (i) the climatic instability originates in ocean dynamics, as it is not observed with the slab, (ii) NH sea ice cover plays a critical role in the shift to the cold climatic mode, (iii) reaching the cold climatic mode requires a lower CO_2 level at 450 Ma than at 470 Ma.

This type of non-linearity within the Earth climate system has been extensively studied in the past few years. We will in particular discuss our results in the light of the major studies from Rose and Marshall (2009) and Ferreira et al. (2011) in Sect. 4, but we propose for now to continue our analysis by focusing on the response of ocean dynamics to the paleogeographical changes occurring between 470 Ma and 450 Ma.

3.2 Sensitivity of ocean dynamics to the paleogeography

Bifurcation from the warm to the cold climatic mode occurs between 12 PAL and 8 PAL at 470 Ma, and between 8 PAL and 6 PAL at 450 Ma. In order to constrain what makes the 450 Ma climatic system more stable, we compare the climatic features at both time slices for a same pCO_2. We use the simulations preceding the tipping-points (12 PAL) to identify the preconditioning factors for the climatic instability. These two simulations have a same global SAT (22.5 °C, Table 1) and a close global ocean temperature (11.1 °C at 470 Ma and 11.4 °C at 450 Ma, Table 1) that make the comparison reasonable.

Figure 6 displays the sea-surface temperatures (SST) for the 470 Ma-12X and the 450 Ma-12X experiments together with the SST difference between these two simulations. From 470 Ma to 450 Ma, the SH cools and the NH warms (Fig. 6c). The temperature changes are on the order of a few degrees, locally up to 3 °C in both hemispheres. Assuming that the NH sea ice extension plays a major role in the abrupt transition from one climatic state to another through the sea ice albedo positive feedback (see Sect. 3.1), the NH warming observed in Fig. 6c appears as the key point accounting

CPD
10, 2767–2804, 2014

for the increasing stability from 470 Ma to 450 Ma. It becomes more difficult to form sea ice and thus to trigger the albedo feedback in the NH through time, and a lower CO_2 concentration is required to enter the cool climatic mode at 450 Ma.

The origin of the temperature pattern observed in Fig. 6c is investigated through the study of the oceanic heat transport (Fig. 7). From 470 Ma to 450 Ma, the NH is marked by a significant increase in the northward OHT exceeding 100 % at 20° N (from 0.4 to 0.8 PW respectively, Fig. 7a). In the SH, a slight decrease in the southward OHT is observed at all latitudes except for a narrow latitudinal band between 6° S and 18° S (Fig. 7a). This new energy redistribution brings more heat to the NH and less to the SH. As a direct consequence, the NH warms from 470 Ma to 450 Ma, and the SH cools.

Dividing the total OHT into its advective and diffusive components (Fig. 7b and c) reveals a striking feature within the NH advective heat transport between ∼ 35° N and ∼ 65° N (Fig. 7b). The transport is negative, meaning a southward heat transport, which is a priori unexpected in the NH. The advective heat transport scales as $\sim \Psi \times \Delta T \times \rho \times C_p$ where Ψ is the strength of the overturning circulation, ΔT the temperature difference between the northward and the southward limbs of the overturning circulation, ρ the water density and C_p the water specific heat. A negative heat transport implies a southward transport of surface warm waters. The southward water flow results from an intense wind-driven eastward circumpolar current that develops at these latitudes in the absence of landmasses (Fig. 8). As a consequence of the Ekman deflection, the water masses are deviated to the right of the main eastward stream and thus constitute a southward mass transport. From 470 Ma to 450 Ma, the northward drift of Siberia (Fig. 8) inhibits the zonal current and the associated Ekman cell, explaining why the reverse OHT weakens through time (Fig. 7b). A similar reverse advective OHT is observed in present-day experiments in the SH due to the Antarctica Circumpolar Current. Figure 7b shows the results obtained for a present-day experiment conducted with a state-of-the-art ocean–atmosphere–vegetation coupled model: the IPSL CM4 GCM (Marti et al., 2010). A reverse heat transport is obtained near 40° S. From this

CPD
10, 2767–2804, 2014

point of view, the Ordovician quasi-oceanic NH keeps some common features with our present-day ∼ 80 % oceanic SH.

The global Northern Hemisphere OHT strengthening, from 470 Ma to 450 Ma (Fig. 7a), is due to an increase of the transport in three main areas (Fig. 9), the location of which turns out to be constrained by changes in the overturning circulation (Fig. 10).

- Between 5° N and 30° N, the advective OHT increases (Fig. 7b) in response to the intensifying surface subtropical cell that directly brings heat from the Equator.
- Between 30° N and ∼ 42° N, the diffusive OHT increases (Fig. 7c) as a consequence of the strengthening of the subtropical cell. Much more heat is "deposited" at 30° N, which imposes a strong temperature gradient. Heat diffuses from the warm tropical latitudes where the heat is "deposited" to the cold waters at higher latitudes.
- Between ∼ 42° N and 60° N, the southward advective OHT weakens through time (Fig. 7b). The northward drift of Siberia inhibits the 40° N zonal current (Fig. 8): the counter-clockwise cell associated to the zonal current acts over the entire water column at 470 Ma and not beyond 2500 m at 450 Ma. Hence less cold waters are brought from the high latitudes to the mid-latitudes resulting in an increased net northward heat transport. An additional process is the deflection of surface warm currents to the North by Siberia at 450 Ma. This can be seen by comparing the isotherms 20 °C and 15 °C in Fig. 6a and b. Although it is restricted to upper levels oceanic waters, this second mechanism is significant because the first tens of meters represent the main heat reservoir of the ocean.

The most significant outstanding issue is to determine why the temperature drawdown occurring through the tipping-point is sharper at 450 Ma than at 470 Ma. Although the tipping-point occurs later at 450 Ma, the two paleogeographical configurations present almost the same global SAT and an equivalent sea ice cover at 6 PAL (Fig. 2 and

CPD
10, 2767–2804, 2014

Table 1). Paradoxically, this sharper response through the 450 Ma tipping-point is due to the paleogeographically-induced increase in the Northern Hemisphere OHT that previously inhibited the cooling. While the NH warms from 470 Ma to 450 Ma (Fig. 6c), the NH equator-to-pole temperature profile flattens (not shown here). These changes are observed within the warm mode at 12 PAL, but they are critical since they constitute the preconditioning factors for the differential climatic sensitivity as climate shifts to the cold climatic mode. The flattened 450 Ma SST gradient delays the tipping-point to a certain extent by inhibiting sea ice growth at polar latitudes, but it increases the global climate sensitivity to the radiative forcing as soon as NH sea ice begins to expand.

4 Discussion

The potential existence of multiple equilibria in the climate system has a long story in the literature. Lorenz (1968) discussed whether the physical laws governing climate are "transitive", supporting a unique climate state, or "intransitive" leading to several sets of long-term statistics. Two main mechanisms supporting climate intransitivity have so far emerged. The first mechanism originates in the study of Stommel (1961) who showed that the thermohaline circulation may sustain two stable regimes depending on whether the driver of the circulation, the density-difference, is dominated by the temperature or the haline gradient, leading respectively to an intense or a weak circulation. This concept motivated later a wealth of studies linking the last glacial abrupt events to these multiple thermohaline states, studies that are today well-known as "fresh water hosing" experiments (see for example Kageyama et al., 2013). The second mechanism is the ice albedo positive feedback. It was independently introduced by Budyko (1969) and Sellers (1969). The authors developped simple one-dimension climate models in which surface temperature is computed by taking into account the local radiative budget and the meridional heat transport. Two stable climate states are obtained for a same solar forcing depending on the initial conditions, describing a classical hysteresis loop: a warm state with a small ice-cap or no ice at all (Eq3, Fig. 11a), and a cold completely

CPD
10, 2767–2804, 2014

ice-covered state (Eq1, Fig. 11a). A large ice-cap of finite size extending to the mid-latitudes constitutes another analytical solution, but this third equilibrium turns out to be very unstable and thus not realizable (Eq2 in Fig. 11a; Rose and Marshall, 2009). Critical non-linearities are observed at both latitudinal extremes (Rose and Marshall, 2009 and references therein). At low latitudes, near the Equator, the "large ice cap instability" rules. An ice margin reaching theses latitudes expands up to the Equator ("snowball" state Eq1, Fig. 11a). At very high latitudes, this is the "small ice cap instability" (SICI): a reduced sea ice cover will either completely disappear or spread until it forms a small ice cap restricted to the high latitudes (warm state, Eq3 in Fig. 11a). In the absence of the equilibrium Eq2, a unique ice cap of large (beyond the SICI domain) but finite (no snowball state) size is obtained for a given climatic forcing (Fig. 11b). A comprehensive review of the successive improvements associated to the energy balance models (EBM) is provided by North et al. (1981).

Recently, Rose and Marshall (2009) managed to stabilize the equilibrium Eq2 by extending the previous EBM through two key processes: (i) the effect by which sea ice insulates the ocean surface from the atmosphere, (ii) the wind-driven structure of the OHT. A primary maximum at low-latitudes accounts for the heat transport by the subtropical gyre and a secondary maximum at high latitudes for the OHT generated by the subpolar gyre, with a local minimum in between (Fig. 11c). Contrary to classical EBM in which the OHT describes a large parabolic curve from the Equator to the Pole (Fig. 11b), the OHT pattern from Rose and Marshall (2009) shows a local minimum at mid-latitudes where the ice edge can stably rest. This OHT structure is closer to the observations (see for example Garnier et al., 2000). Within the improved EBM of Rose and Marshall (2009), the SICI does not exist anymore: ice caps of various size can persist at polar latitudes. Because the equilibrium Eq2 is now stable, two ice caps of large but finite size can be sustained for a same climatic forcing (e.g., for F5 in Fig. 11c). The position of the sea ice edge in the equilibrium Eq2 is slaved to the position of the mid-latitude OHT minimum and thus very stable when external forcing is varied.

CPD
10, 2767–2804, 2014

The question however still remained if the mid-latitude equilibrium Eq2 would hold in a more complex climate model with many degrees of freedom and a strong internal variability. Ferreira et al. (2011) demonstrated multiple equilibria using an up-to-date ocean GCM (the MITgcm) on two idealized configurations: a purely aqua planet, and an ocean planet with a strip of land extending from one pole to the other. The three states from Rose and Marshall (2009) are obtained: (i) a warm, ice-free state, (ii) a cold state with sea ice extending down to mid-latitudes, (iii) and the completely ice-covered "snowball" state. The authors highlight the consistency of their results with the study of Rose and Marshall (2009). In their complex GCM, the multiple equilibria owe their existence to the latitudinal structure of the OHT. The authors moreover extend the previous results from Rose and Marshall (2009) by demonstrating that no OHT minimum is required. A weak high-latitude OHT within the subpolar gyre is sufficient to stabilize a finite ice cap at mid-latitudes, in that critical weak-OHT zone situated between the subtropical and the subpolar gyres that they widely refer to as the "OHT convergence".

Here, we have investigated the Ordovician climate sensitivity to a varying radiative forcing. The hallmark of our results is the existence of a global climatic instability in the NH. A tipping-point separates two climatic modes: a warm mode with no sea ice in the NH, and a cold mode with sea ice extending down to the mid-latitudes (Fig. 5a). In the light of the results from Rose and Marshall (2009) and Ferreira et al. (2011), these climatic modes respectively correspond to the classical warm mode obtained with an EBM and to the third equilibrium previously described, respectively Eq3 and Eq2 in Fig. 11. The simulations marked by a weak pCO_2 stabilize in Eq2, whereas the experiments conducted with high CO_2 levels lead to the warm state Eq3.

It is noteworthy that the latitudinal position at which the sea ice edge stabilizes within the cold climatic mode effectively lies immediatly poleward of the Northern Hemisphere OHT convergence (Fig. 12, $\sim 40^{\circ}$ N), which is a key prediction from Rose and Marshall (2009) and Ferreira et al. (2011). According to these authors, the strong low-latitude OHT encounters here a weaker transport and heat is "deposited", thus preventing the ice edge from moving further equatorward.

CPD
10, 2767–2804, 2014

The fact that the ice edge is strongly slaved to the OHT convergence (Fig. 12; Rose and Marshall, 2009) explains why the model returns to its initial sensitivity below 4 PAL (see Sect. 3.1). Ice cannot spread further and stabilizes. The sea ice albedo feedback is geometrically stopped by the subtropical high-OHT barrier and cooling is consequently slowed-down.

The comparison of Fig. 11b and c permits to explain why tipping-points were not previously observed for the Ordovician. Similarly to the classical EBM, the slab models use a purely diffusive transport. The resulting OHT describes the same large parabolic curve from the Equator to the Pole (Fig. 12). There is no OHT minimum or more largely no OHT convergence where the sea ice edge could rest to make the mid-latitude equilibrium stable. Climate cannot switch between stable states which inhibits the climatic instability.

Besides, the similarity between EBM and slab models explains the results from Gibbs et al. (1997) who observed with the slab model GENESIS a runaway icehouse that they interpreted as resulting from the SICI. As it was previously explained, this mechanism is not observed anymore when the OHT structure is taken into account, but it is a classical feature of the EBM and by extension of all models that use a diffusive OHT. We emphasize that the runaway icehouse proposed by Gibbs et al. (1997) and the climatic instability suggested in this study rely on much different mechanisms.

The absence of ocean dynamics in the slab models makes their response to an atmospheric forcing much different from the ocean–atmosphere GCM when simulating time periods of particular land–sea configuration as it is the case for the Ordovician. An efficient way to overcome that apparent deficiency would be to impose the structure of the latitudinal OHT, as Rose and Marshall (2009) did in their extended EBM. The decisive answer is brought by Ferreira et al. (2011), who tested this hypothesis within the MITgcm used as a slab. With the simple diffusive coefficient, the mid-latitude equilibrium is not stable, as for classical EBM. However, by imposing the OHT deduced from their coupled runs to the slab, they managed to reproduce exactly the same climatic response as with their complex GCM. These results definitely prove that the differential

CPD
10, 2767–2804, 2014

behaviour of ocean–atmosphere and slab–atmosphere GCM lies within ocean dynamics through the OHT.

The Ordovician Time Period turned out to bring a favorable paleogeographical context to propose the sudden shift between different climate states on a realistic configuration. The stabilization of a sea ice edge at mid-latitudes requires a wind-driven latitudinal OHT structure, a condition that can be reached only in an oceanic context. It is notably the case of the Ordovician 95 % oceanic NH which ocean zonal circulation is not hampered by continental masses. If continents were largely distributed at all latitudes, then continental edges would strongly alter the pattern originally imposed by the winds and by the Ekman pumping mechanism. The OHT may thus be more even at all latitudes, as it is the case in our study in the SH due to the supercontinent Gondwana (Figs. 1 and 12). No OHT convergence would be obtained and the OHT pattern would become very similar to the one imposed by a simple diffusion coefficient. From this point of view, it is logical that the global instability lies in our study in the oceanic NH, and it would anyway be inconceivable to obtain a similar behaviour in the SH.

5 Conclusion

We have examined the response of the Ordovician climate to a decreasing pCO_2 for two continental configurations at 470 Ma and at 450 Ma with the coupled ocean, atmosphere and sea ice GCM FOAM. We have found the existence of tipping-points in the Ordovician climate owing to the peculiar paleogeography with a quasi-oceanic Northern Hemisphere. As a result, the climate may have abruptly shifted from a warm climatic mode to a cold climatic mode. Warm SST and no sea ice in the NH characterize the warm mode, whereas much colder SST and a large sea ice extension till the mid-latitudes mark the cool mode. We also note that subtle changes occurring in the continental configuration between 470 and 450 Ma make the latter less sensitive to the radiative forcing. Indeed, the bifurcation point from the warm to the cold climatic mode takes place between 12 PAL and 8 PAL at 470 Ma, and between 8 PAL and

CPD
10, 2767–2804, 2014

6 PAL at 450 Ma. One potential mechanism relies on the changes occurring in the ocean heat transport between the two simulated time periods. The paleogeographical evolution promotes a larger northward oceanic heat transport at 450 Ma which in turn induces warmer Northern Hemisphere SST. Spread of sea ice becomes more difficult and a lower CO_2 level is required to enter the cold climatic mode.

The tipping point is due to a climatic instability occurring in the quasi-oceanic Northern Hemisphere. The instability relies on the brutal shift from a warm climate to a climatic equilibrium characterised by a sea ice front resting at mid-latitudes. This particular climate state has been widely discussed in the literature and proven to require a wind-driven latitudinal structure of the OHT (Rose and Marshall, 2009; Ferreira et al., 2011). The classical EBM and slab models use a purely diffusive OHT and are by construction unable to stabilize an ice edge at the mid-latitudes (Rose and Marshall, 2009; Ferreira et al., 2011), explaining why that behaviour was never noticed in previous studies about the Ordovician climate (e.g., Gibbs et al., 1997; Herrmann et al., 2004b). Published studies performed with idealized land–sea configurations however demonstrate that this limitation may be overcome by imposing a latitudinally varied diffusion coefficient reproducing the OHT structure. Such extended EBM and slab models successfully reproduce the behaviour of the more complex ocean–atmosphere GCM (Rose and Marshall, 2009; Ferreira et al., 2011).

The Late Ordovician glaciation is a particular time in Earth History since it occurred under otherwise warm climatic conditions marked by high CO_2 levels. Although the Faint Young Sun somewhat reduces this discrepancy between high CO_2 and glacial onset, the best hypotheses to trigger the Ordovician glaciation require today a Late Ordovician drop in CO_2. In particular, recent geochemical data suggest an abrupt tropical SST cooling during the Hirnantian (Trotter et al., 2008; Finnegan et al., 2011) associated to the rapid growth of large ice-sheets (Finnegan et al., 2011). Several CO_2 sinks have been proposed to explain that cooling but no consensus has been found so far (Brenchley et al., 1994; Kump et al., 1999; Villas et al., 2002; Lenton et al., 2012). In this context, the tipping-point becomes a very interesting working hypothesis. It requires

CPD
10, 2767–2804, 2014

only a slight CO_2 decrease and at the same time induces a sharp global temperature drawdown. The climatic instability demonstrated in this study therefore represents a step forward in understanding the Ordovician glacial events and provides in particular a minimal hypothesis for the Hirnantian abrupt cooling and associated glacial pulse.

Acknowledgements. This work was granted access to the HPC resources of TGCC under the allocation 2014-012212 made by GENCI. The authors thank Pierre Sepulchre for providing the IPSL CM4 GCM run. We are also grateful to David G. Ferreira for his constructive and helpful comments.

References

Berner, R. A.: GEOCARBSULF: a combined model for Phanerozoic atmospheric O_2 and CO_2, Geochim. Cosmochim. Ac., 70, 5653–5664, doi:10.1016/j.gca.2005.11.032, 2006.

Berner, R. A. and Kothavala, Z.: GEOCARB III: a revised model of atmospheric CO_2 over Phanerozoic time, Am. J. Sci., 301, 182–204, doi:10.2475/ajs.301.2.182, 2001.

Beuf, S., Biju-Duval, B., De Charpal, O., Rognon, P., Gariel, O., and Bennacef, A.: Les grès du Paléozoïque Inférieur au Sahara, Technip, Paris, 464 pp., 1971.

Blakey, R. C.: Carboniferous–Permian paleogeography of the assembly of Pangea, in: Fifteenth International Congress on Carboniferous and Permian Stratigraphy, edited by: Wong, T. E., Utrecht, the Netherlands, pages 443–465, Royal Netherlands Academy of Arts and Sciences, Amsterdam, 2007.

Braconnot, P., Harrison, S. P., Kageyama, M., Bartlein, P. J., Masson-Delmotte, V., Abe-Ouchi, A., Otto-Bliesner, B., and Zhao, Y.: Evaluation of climate models using palaeoclimatic data, Nat. Clim. Change, 2, 417–424, doi:10.1038/NCLIMATE1456, 2012.

Brenchley, P. J., Marshall, J. D., Carden, G., Robertson, D., Long, D., Meidla, T., Hints, L., and Anderson, T. F.: Bathymetric and isotopic evidence for a short-lived Late Ordovician glaciation in a greenhouse period, Geology, 22, 295–298, doi:10.1130/0091-7613(1994)022<0295:BAIEFA>2.3.CO;2, 1994.

Brenchley, P. J., Carden, G. A., Hints, L., Kaljo, D., Marshall, J. D., Martma, T., Meidla, T., and Nõlvak, J.: High-resolution stable isotope stratigraphy of Upper Ordovician sequences: constraints on the timing of bioevents and environmental changes associated

CPD
10, 2767–2804, 2014

with mass extinction and glaciation, Geol. Soc. Am. Bull., 115, 89–104, doi:10.1130/0016-7606(2003)115<0089:HRSISO>2.0.CO;2, 2003.
Budyko, M. I.: The effect of solar radiation variations on the climate of the earth, Tellus, 21, 611–619, 1969.
Crowley, T. J. and Baum, S. K.: Toward reconciliation of Late Ordovician (~ 440 Ma) glaciation with very high CO_2 levels, J. Geophys. Res.-Atmos., 96, 22597–22610, doi:10.1029/91JD02449, 1991.
Crowley, T. J. and Baum, S. K.: Modeling late Paleozoic glaciation, Geology, 2, 507–510, doi:10.1130/0091-7613(1992)020<0507:MLPG>2.3.CO;2, 1992.
Crowley, T. J. and Baum, S. K.: Reconciling Late Ordovician (440 Ma) glaciation with very high (14X) CO_2 levels, J. Geophys. Res.-Atmos., 100, 1093–1101, doi:10.1029/94JD02521, 1995.
Crowley, T. J., Baum, S. K., and Kim, K. Y.: General circulation model sensitivity experiments with pole-centered supercontinents, J. Geophys. Res.-Atmos., 98, 8793–8800, doi:10.1029/93JD00122, 1993.
Denis, M., Buoncristiani, J.-F., Konate, M., Ghienne, J.-F., and Guiraud, M.: Hirnantian glacial and deglacial record in SW Djado Basin (NE Niger), Geodin. Acta, 20, 177–195, doi:10.3166/ga.20.177-195, 2007.
Dera, G. and Donnadieu, Y.: Modeling evidences for global warming, Arctic seawater freshening, and sluggish oceanic circulation during the Early Toarcian anoxic event, Paleoceanography, 27, PA2211, doi:10.1029/2012PA002283, 2012.
Díaz-Martínez, E. and Grahn, Y.: Early Silurian glaciation along the western margin of Gondwana (Peru, Bolivia and northern Argentina): Palaeogeographic and geodynamic setting, Palaeogeogr. Palaeocl., 245, 62–81, doi:10.1016/j.palaeo.2006.02.018, 2007.
Donnadieu, Y., Goddéris, Y., and Bouttes, N.: Exploring the climatic impact of the continental vegetation on the Mezosoic atmospheric CO_2 and climate history, Clim. Past, 5, 85–96, doi:10.5194/cp-5-85-2009, 2009.
Endal, A. S. and Sofia, S.: Rotation in solar-type stars, I – Evolutionary models for the spin-down of the sun, Astrophys. J., 243, 625–640, 1981.
Ferreira, D., Marshall, J., and Rose, B.: Climate determinism revisited: multiple equilibria in a complex climate model, J. Climate, 24, 992–1012, doi:10.1175/2010JCLI3580.1, 2011.

CPD
10, 2767–2804, 2014

Finnegan, S., Bergmann, K., Eiler, J. M., Jones, D. S., Fike, D. A., Eisenman, I., Hughes, N. C., Tripati, A. K., and Fischer, W. W.: The magnitude and duration of Late Ordovician-Early Silurian glaciation, Science, 331, 903–906, doi:10.1126/science.1200803, 2011.

Garnier, E., Barnier, B., Siefridt, L., and Béranger, K.: Investigating the 15 years air–sea flux climatology from the ECMWF re-analysis project as a surface boundary condition for ocean models, Int. J. Climatol., 20, 1653–1673, doi:10.1002/1097-0088(20001130)20:14<1653::AID-JOC575>3.0.CO;2-G, 2000.

Ghienne, J.-F., Le Heron, D., Moreau, J., Denis, M., and Deynoux, M.: The Late Ordovician glacial sedimentary system of the North Gondwana platform, in: Glacial Sedimentary Processes and Products, Special Publication, edited by: Hambrey, M., Christoffersen, P., Glasser, N., Janssen, P., Hubbard, B., and Siegert, M., 39, 295–319, International Association of Sedimentologists, Blackwells, Oxford, 2007.

Gibbs, M. T., Barron, E. J., and Kump, L. R.: An atmospheric pCO_2 threshold for glaciation in the Late Ordovician, Geology, 25, 447–450, doi:10.1130/0091-7613(1997)025<0447:AAPCTF>2.3.CO;2, 1997.

Gough, D. O.: Solar interior structure and luminosity variations, Sol. Phys., 74, 21–34, 1981.

Herrmann, A. D., Patzkowsky, M. E., and Pollard, D.: Obliquity forcing with 8–12 times preindustrial levels of atmospheric pCO_2 during the Late Ordovician glaciation, Geology, 31, 485–488, doi:10.1130/0091-7613(2003)031<0485:OFWTPL>2.0.CO;2, 2003.

Herrmann, A. D., Haupt, B. J., Patzkowsky, M. E., Seidov, D., and Slingerland, R. L.: Response of Late Ordovician paleoceanography to changes in sea level, continental drift, and atmospheric pCO_2: potential causes for long-term cooling and glaciation, Palaeogeogr. Palaeocl., 210, 385–401, doi:10.1016/j.palaeo.2004.02.034, 2004a.

Herrmann, A. D., Patzkowsky, M. E., and Pollard, D.: The impact of paleogeography, pCO_2, poleward ocean heat transport and sea level change on global cooling during the Late Ordovician, Palaeogeogr. Palaeocl., 206, 59–74, doi:10.1016/j.palaeo.2003.12.019, 2004b.

International Commission on Stratigraphy: International Chronostratigraphic Chart v2014/02, available at: www.stratigraphy.org, 2014.

IPCC: Climate Change 2013: The physical science basis, in: Contribution of Working Group I to the Fifth Assessment Report of the Intergovernmental Panel on Climate Change, edited by: Stocker, T. F., Qin, D., Plattner, G.-K., Tignor, M., Allen, S. K., Boschung, J., Nauels, A., Xia, Y., Bex, V., and Midgley, P. M., Cambridge University Press, Cambridge, UK and New York, NY, USA, 1535 pp., 2013.

CPD
10, 2767–2804, 2014

Jacob, R. L.: Low frequency variability in a simulated atmosphere ocean system, Ph.D. thesis, University of Wisconsin-Madison, 1997.

Kageyama, M., Merkel, U., Otto-Bliesner, B., Prange, M., Abe-Ouchi, A., Lohmann, G., Ohgaito, R., Roche, D. M., Singarayer, J., Swingedouw, D., and Zhang, X.: Climatic impacts of fresh water hosing under Last Glacial Maximum conditions: a multi-model study, Clim. Past, 9, 935–953, doi:10.5194/cp-9-935-2013, 2013.

Kiehl, J. T., Hack, J. J., Bonan, G. B., Boville, B. A., Williamson, D. L., and Rasch, P. J.: The national center for Atmospheric Research community climate model: CCM3, J. Climate, 11, 1131–1149, doi:10.1175/1520-0442(1998)011<1131:TNCFAR>2.0.CO;2, 1998.

Kothavala, Z., Oglesby, R. J., and Saltzman, B.: Sensitivity of equilibrium surface temperature of CCM3 to systematic changes in atmospheric CO_2, Geophys. Res. Lett., 26, 209–212, doi:10.1029/1998GL900275, 1999.

Kump, L. R., Arthur, M. A., Patzkowsky, M. E., Gibbs, M. T., Pinkus, D. S., and Sheehan, P. M.: A weathering hypothesis for glaciation at high atmospheric pCO_2 during the Late Ordovician, Palaeogeogr. Palaeocl., 152, 173–187, doi:10.1016/S0031-0182(99)00046-2, 1999.

Lefebvre, V., Donnadieu, Y., Sepulchre, P., Swingedouw, D., and Zhang, Z.-S.: Deciphering the role of southern gateways and carbon dioxide on the onset of the Antarctic Circumpolar Current, Paleoceanography, 27, PA4201, doi:10.1029/2012PA002345, 2012.

Lenton, T. M., Crouch, M., Johnson, M., Pires, N., and Dolan, L.: First plants cooled the Ordovician, Nat. Geosci., 5, 86–89, doi:10.1038/ngeo1390, 2012.

Loi, A., Ghienne, J.-F., Dabard, M. P., Paris, F., Botquelen, A., Christ, N., Elaouad-Debbaj, Z., Gorini, A., Vidal, M., Videt, B., and Destombes, J.: The Late Ordovician glacio-eustatic record from a high-latitude storm-dominated shelf succession: the Bou Ingarf section (Anti-Atlas, Southern Morocco), Palaeogeogr. Palaeocl., 296, 332–358, doi:10.1016/j.palaeo.2010.01.018, 2010.

Lorenz, E. N.: Climatic determinism, Meteor. Mon., 8, 1–3, 1968.

Marti, O., Braconnot, P., Dufresne, J. L., Bellier, J., Benshila, R., Bony, S., Brockmann, P., Cadule, P., Caubel, A., Codron, F., Noblet, N., Denvil, S., Fairhead, L., Fichefet, T., Foujols, M. A., Friedlingstein, P., Goosse, H., Grandpeix, J. Y., Guilyardi, E., Hourdin, F., Idelkadi, A., Kageyama, M., Krinner, G., Lévy, C., Madec, G., Mignot, J., Musat, I., Swingedouw, D., and Talandier, C.: Key features of the IPSL ocean atmosphere model and its sensitivity to atmospheric resolution, Clim. Dynam., 34, 1–26, doi:10.1007/s00382-009-0640-6, 2010.

CPD
10, 2767–2804, 2014

Nardin, E., Goddéris, Y., Donnadieu, Y., Le Hir, G., Blakey, R. C., Pucéat, E., and Aretz, M.: Modeling the early Paleozoic long-term climatic trend, Geol. Soc. Am. Bull., 123, 1181–1192, doi:10.1130/B30364.1, 2011.
North, G. R., Cahalan, R. F., and Coakley, J. A.: Energy balance climate models, Rev. Geophys., 19, 91–121, 80R1502, doi:10.1029/RG019i001p00091, 1981.
Pancost, R. D., Freeman, K. H., Herrmann, A. D., Patzkowsky, M. E., Ainsaar, L., and Martma, T.: Reconstructing Late Ordovician carbon cycle variations, Geochim. Cosmochim. Ac., 105, 433–454, doi:10.1016/j.gca.2012.11.033, 2013.
Poulsen, C. J. and Jacob, R. L.: Factors that inhibit snowball Earth simulation, Paleoceanography, 19, PA4021, doi:10.1029/2004PA001056, 2004.
Poussart, P. F., Weaver, A. J., and Barnes, C. R.: Late Ordovician glaciation under high atmospheric CO_2: a coupled model analysis, Paleoceanography, 14, 542–558, doi:10.1029/1999PA900021, 1999.
Rose, B. E. J. and Marshall, J.: Ocean heat transport, sea ice, and multiple climate states: insights from energy balance models, J. Atmos. Sci., 66, 2828–2843, doi:10.1175/2009JAS3039.1, 2009.
Rubinstein, C. V., Gerrienne, P., de la Puente, G. S., Astini, R. A., and Steemans, P.: Early Middle Ordovician evidence for land plants in Argentina (eastern Gondwana), New Phytol., 188, 365–369, doi:10.1111/j.1469-8137.2010.03433.x, 2010.
Saltzman, M. R. and Young, S. A.: Long-lived glaciation in the Late Ordovician? Isotopic and sequence-stratigraphic evidence from western Laurentia, Geology, 33, 109–112, doi:10.1130/G21219.1, 2005.
Sellers, W. D.: A global climatic model based on the energy balance of the earth-atmosphere system, J. Appl. Meteorol., 8, 392–400, doi:10.1175/1520-0450(1969)008<0392:AGCMBO>2.0.CO;2, 1969.
Semtner, Jr, A. J.: A model for the thermodynamic growth of sea ice in numerical investigations of climate, J. Phys. Oceanogr., 6, 379–389, doi:10.1175/1520-0485(1976)006<0379:AMFTTG>2.0.CO;2, 1976.
Servais, T., Owen, A. W., Harper, D. A., Kröger, B., and Munnecke, A.: The Great Ordovician Biodiversification Event (GOBE): the palaeoecological dimension, Palaeogeogr. Palaeocl., 294, 99–119, doi:10.1016/j.palaeo.2010.05.031, 2010.
Sheehan, P. M.: The late Ordovician mass extinction, Annu. Rev. Earth Pl. Sci., 29, 331–364, doi:10.1146/annurev.earth.29.1.331, 2001.

CPD
10, 2767–2804, 2014

Spjeldnaes, N.: Ordovician climatic zones, Norsk Geol. Tidsskr., 41, 45–77, 1962.
Steemans, P., Le Herissé, A., Melvin, J., Miller, M. A., Paris, F., Verniers, J., and Wellman, C. H.: Origin and radiation of the earliest vascular land plants, Science, 324, 353–353, doi:10.1126/science.1169659, 2009.
Stommel, H.: Thermohaline convection with two stable regimes of flow, Tellus, 13, 224–230, 1961.
Sutcliffe, O. E., Dowdeswell, J. A., Whittington, R. J., Theron, J. N., and Craig, J.: Calibrating the Late Ordovician glaciation and mass extinction by the eccentricity cycles of Earth's orbit, Geology, 28, 967–970, doi:10.1130/0091-7613(2000)28<967:CTLOGA>2.0.CO;2, 2000.
Trotter, J. A., Williams, I. S., Barnes, C. R., Lécuyer, C., and Nicoll, R. S.: Did cooling oceans trigger Ordovician biodiversification? Evidence from conodont thermometry, Science, 321, 550–554, doi:10.1126/science.1155814, 2008.
Turner, B. R., Armstrong, H. A., Wilson, C. R., and Makhlouf, I. M.: High frequency eustatic sea-level changes during the Middle to early Late Ordovician of southern Jordan: Indirect evidence for a Darriwilian Ice Age in Gondwana, Sediment. Geol., 251, 34–48, doi:10.1016/j.sedgeo.2012.01.002, 2012.
Vandenbroucke, T. R., Armstrong, H. A., Williams, M., Paris, F., Zalasiewicz, J. A., Sabbe, K., Nõlvak, J., Challands, T. J., Verniers, J., and Servais, T.: Polar front shift and atmospheric CO_2 during the glacial maximum of the Early Paleozoic Icehouse. P. Natl. Acad. Sci., 107, 14983–14986, doi:10.1073/pnas.1003220107, 2010.
Villas, E., Vennin, E., Álvaro, J. J., Hammann, W., Herrera, Z. A., and Piovano, E. L.: The late Ordovician carbonate sedimentation as a major triggering factor of the Hirnantian glaciation, B. Soc. Geol. Fr., 173, 569–578, doi:10.2113/173.6.569, 2002.
Yapp, C. J. and Poths, H.: Ancient atmospheric CO_2 pressures inferred from natural goethites, Nature, 355, 342–344, doi:10.1038/355342a0, 1992.
Young, G. M., Minter, W., and Theron, J. N.: Geochemistry and palaeogeography of upper Ordovician glaciogenic sedimentary rocks in the Table Mountain Group, South Africa, Palaeogeogr. Palaeocl., 214, 323–345, doi:10.1016/j.palaeo.2004.07.029, 2004.
Zhang, Z.-S., Yan, Q., and Wang, H.-J.: Has the Drake passage played an essential role in the Cenozoic cooling?, Atmos. Ocean. Sci. Lett., 3, 288–292, 2010.

CPD
10, 2767–2804, 2014

Table 1. Overview of the simulations. The name of each experiment includes the age of the paleogeography used in input followed by the pCO_2 expressed in PAL. These abbreviations are used throughout the manuscript. Slab runs are not shown.

Simulations	pCO_2 (ppm)	Surface air temperature (°C)	Global temperature of the Ocean (°C)	Mean annual global sea ice cover (10^6 km^2)	Mean annual Southern Hemisphere sea ice cover (10^6 km^2)	Mean annual Northern Hemisphere sea ice cover (10^6 km^2)
450 Ma–2X	560	−0.3	1.8	123.9	49.3	74.6
450 Ma–4X	1120	4.5	2.5	105.1	35.2	69.9
450 Ma–6X	1680	12.1	4.1	58.5	15.5	43.0
450 Ma–8X	2240	20.8	9.0	1.8	1.8	0.0
450 Ma–12X	3360	22.5	11.4	1.1	1.1	0.0
450 Ma–16X	4480	23.7	12.7	0.9	0.9	0.0
470 Ma–2X	560	4.7	2.3	102.3	28.3	74.0
470 Ma–4X	1120	8.6	3.1	85.4	19.2	66.2
470 Ma–6X	1680	11.8	3.9	63.1	10.9	52.2
470 Ma–8X	2240	16.7	6.7	26.0	3,2	22.8
470 Ma–12X	3360	22.5	11.1	0.3	0.3	0.0
470 Ma–16X	4480	23.5	12.0	0.4	0.4	0.0

CPD
10, 2767–2804, 2014

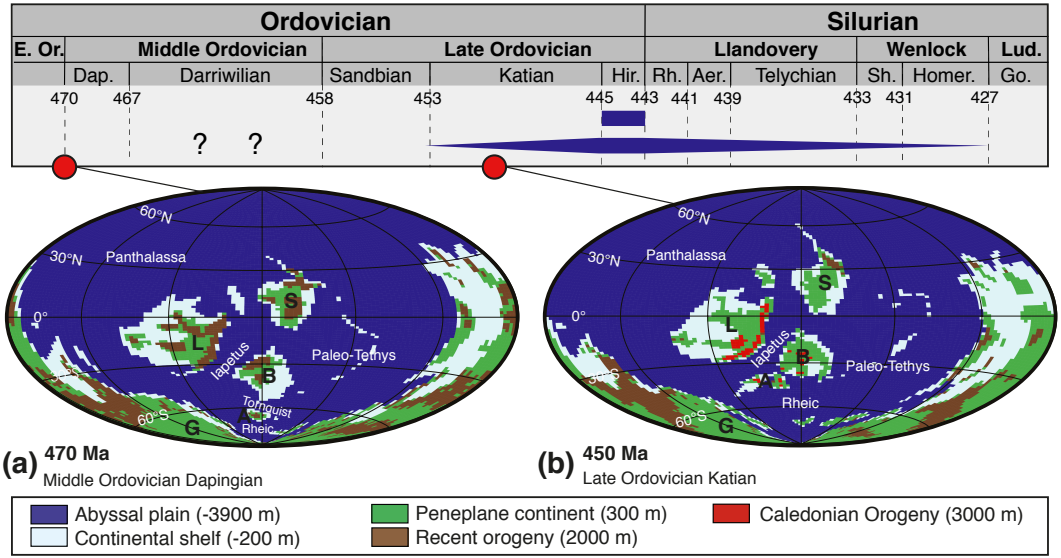

Figure 1. Continental configurations with the FOAM ocean grid based on the paleogeographical reconstructions from Blakey (2007), with the color code for the bathymetric and topographic categories used in this study. *G: Gondwana*, *A: Avalonia*, *B: Baltica*, *L: Laurentia*, *S: Siberia*. Ocean names are in italic. Each time slice is replaced on the synthetic Ordovician glaciation chronology (inspired from Finnegan et al., 2011). Age limits are taken from the geological time scale v2014/02 (International Commission on Stratigraphy, 2014). Question marks are time intervals when hypothetical first ice-sheets may have appeared according to Turner et al. (2012).

CPD
10, 2767–2804, 2014

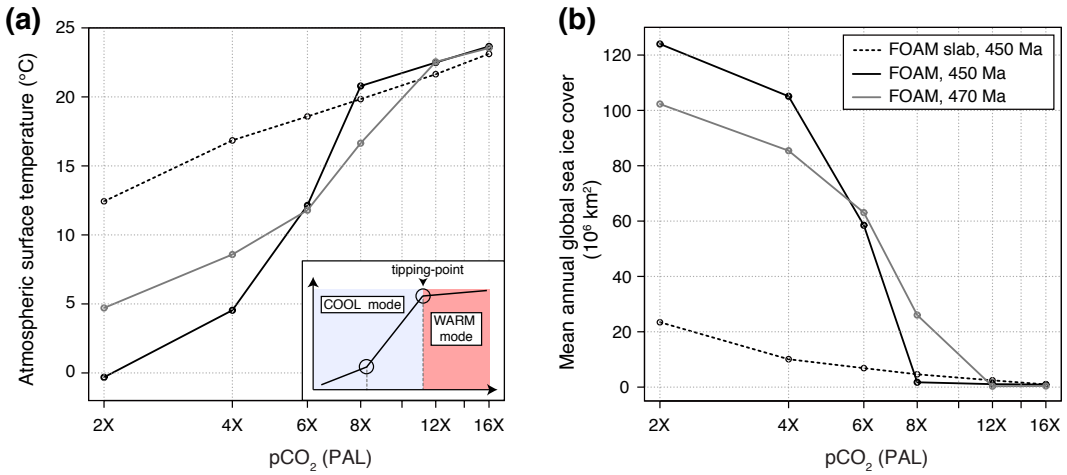

Figure 2. (a) Mean annual, globally-averaged surface air temperature for various pCO_2 values from 2 PAL to 16 PAL, with the slab-version of FOAM at 450 Ma and with the fully coupled ocean–atmosphere-sea ice version of FOAM at 470 Ma and at 450 Ma. The sketch illustrates the explanations provided in the main text. Note the logarithmic scale on the x-axis. **(b)** Same plot as **(a)**, for the mean annual global sea ice cover expressed in Mkm^2.

CPD
10, 2767–2804, 2014

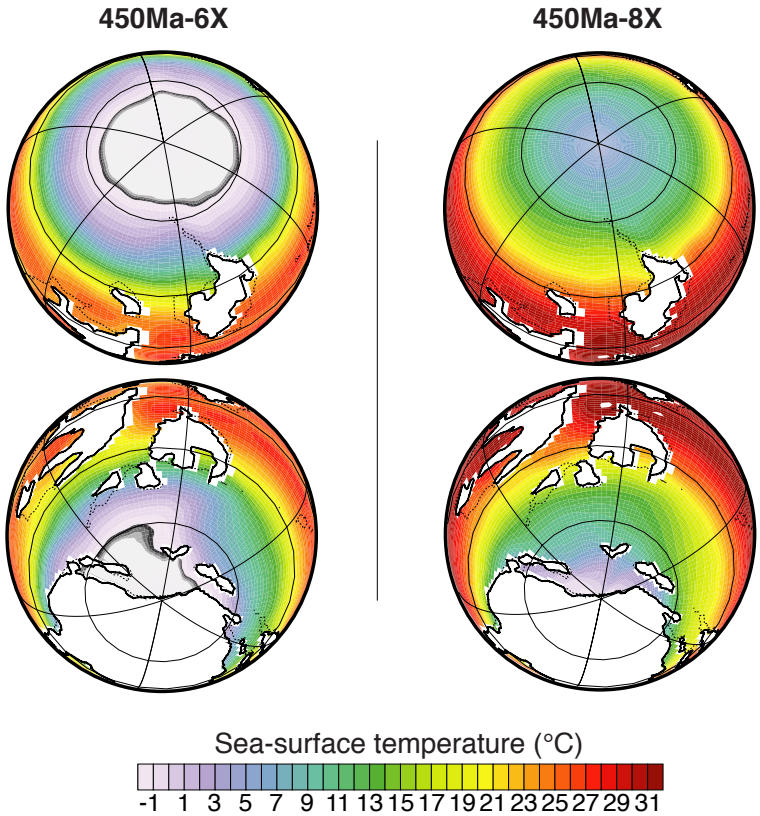

Figure 3. SST (color shading) and permanent sea ice cover (black-and-white shading) at 450 Ma within the cold climatic mode (at 6 PAL) and within the warm climatic mode (at 8 PAL). The permanent sea ice cover is defined as the sum of all grid points whose at least 80 % of the surface is covered by sea ice during a year, allowing to discard temporary sea ice cover by icebergs or rapidly advancing and retreating ice-fronts. Solid contours indicate the coastline, dashed contours indicate the continental plateau distal edge.

CPD
10, 2767–2804, 2014

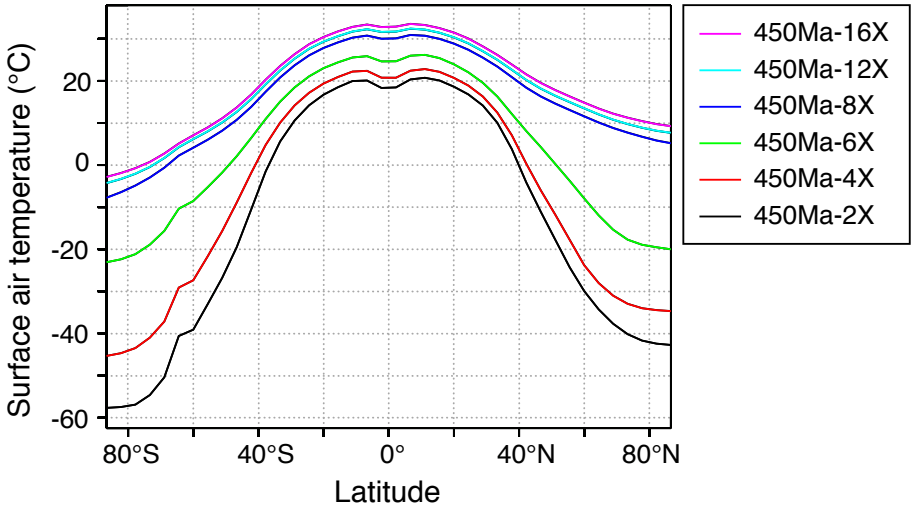

Figure 4. Mean annual, zonally averaged SAT for each pCO_2 at 450 Ma.

CPD
10, 2767–2804, 2014

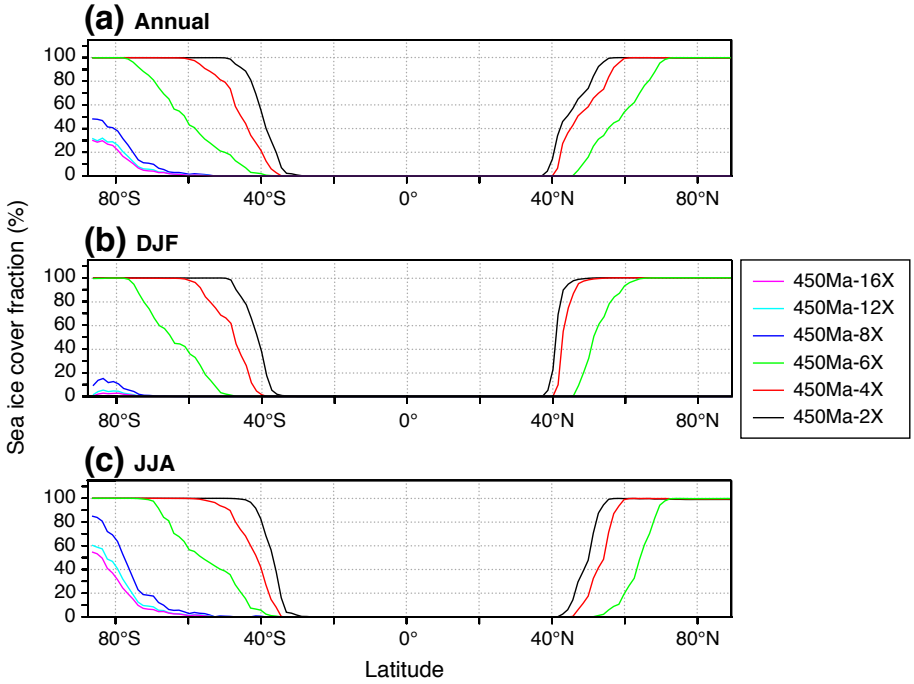

Figure 5. Zonally averaged sea ice cover fraction expressed in percents for each pCO_2 at 450 Ma. *DJF: December, January and February. JJA: June, July and August.*

CPD
10, 2767–2804, 2014

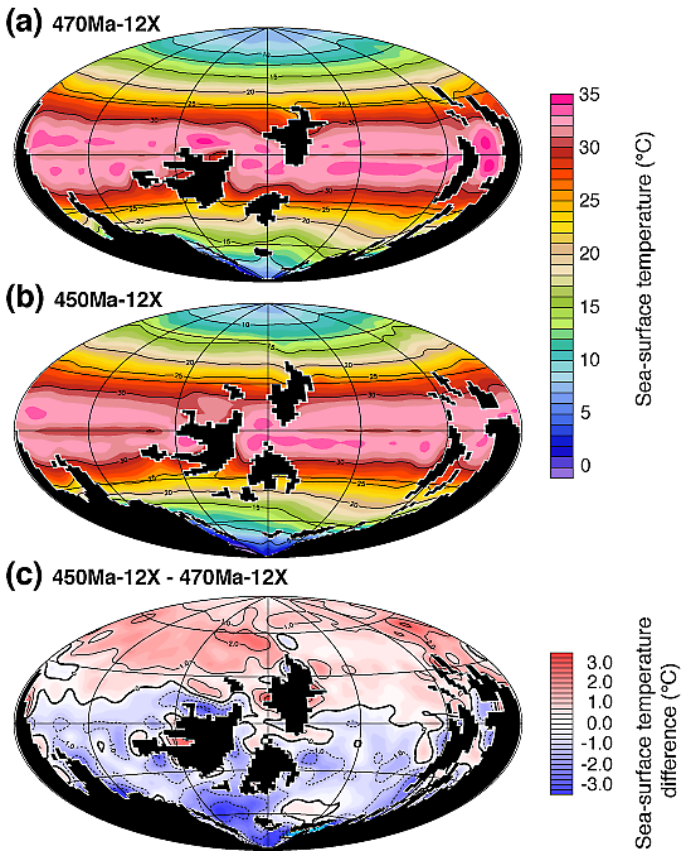

Figure 6. Comparison of the SST at 12 PAL for the two continental configurations used in this study. The black mask stands for continental masses. Note that, for the plot presented in **(c)**, the mask actually represents all the grid points where the SST difference could not be calculated, cumulating each point that is a continent either in the 450 Ma or in the 470 Ma configuration.

CPD
10, 2767–2804, 2014

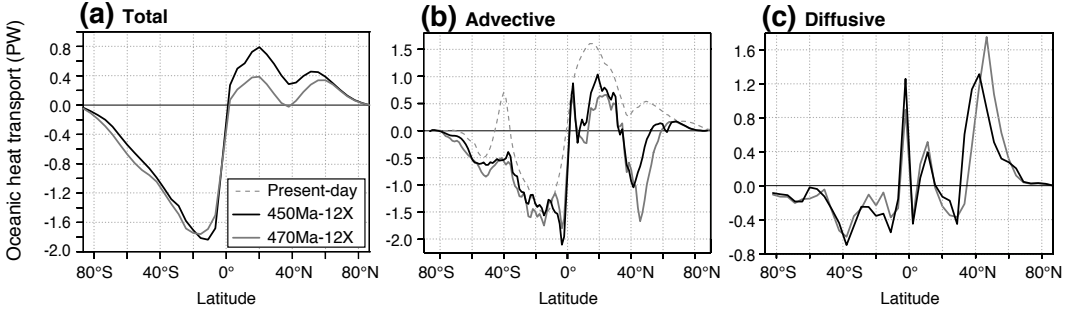

Figure 7. Comparison of the total, advective and diffusive OHT at 12 PAL for the two continental configurations used in this study. The OHT is given in PetaWatts (1 PW = 10^{15} W). The present-day curve is the control experiment conducted at present-day conditions with the up-to-date IPSL CM4 GCM (see the main text for explanations).

CPD
10, 2767–2804, 2014

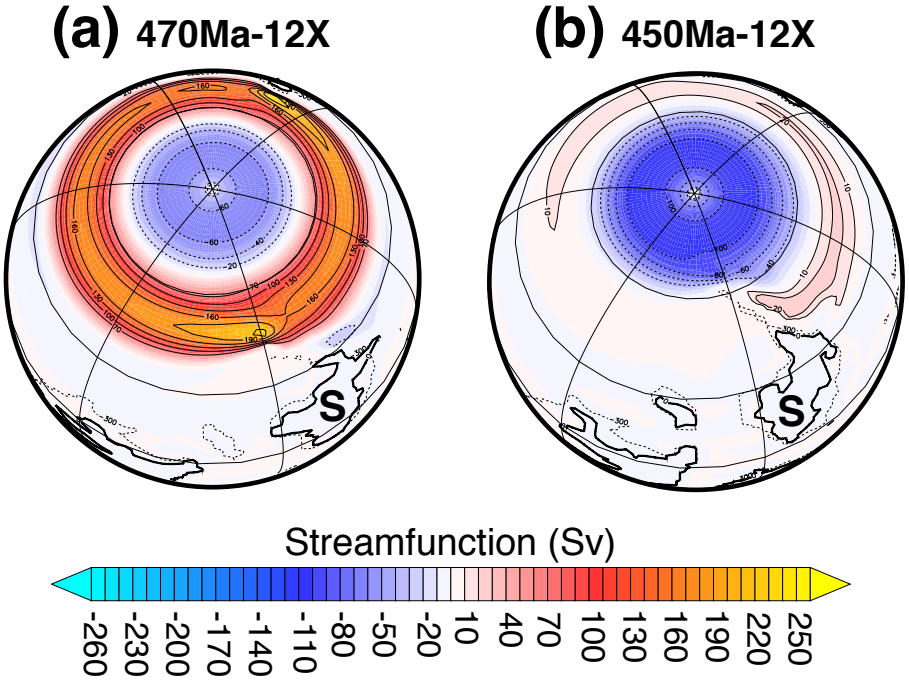

Figure 8. Siberia's northward drift and the consequences on the longitudinal streamfunction. Eastward stream is positive (red), westward stream is negative (blue). The streamfunction is integrated over the whole water column. *S: Siberia*.

CPD
10, 2767–2804, 2014

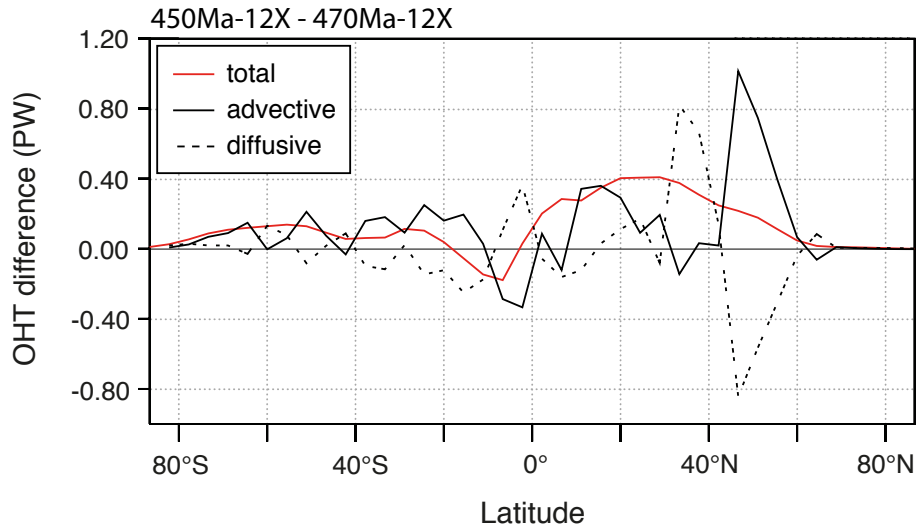

Figure 9. Difference in total, advective and diffusive OHT between the 450 Ma-12X and the 470 Ma-12X simulations.

CPD
10, 2767–2804, 2014

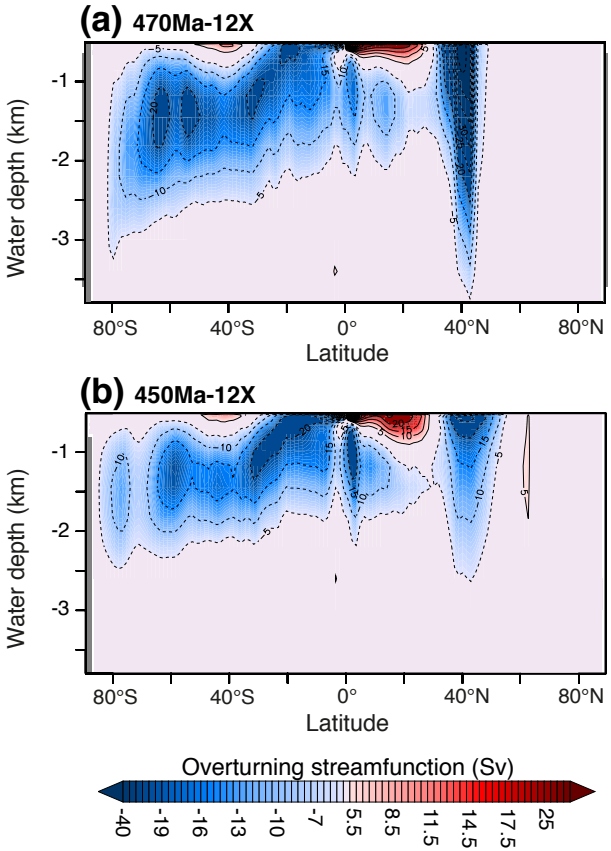

Figure 10. Comparison of the global meridional overturning circulation at 12 PAL for the two continental configurations used in this study. Red shading and solid contours indicate a clockwise circulation, blue shading and dashed contours indicate a counter-clockwise circulation.

CPD
10, 2767–2804, 2014

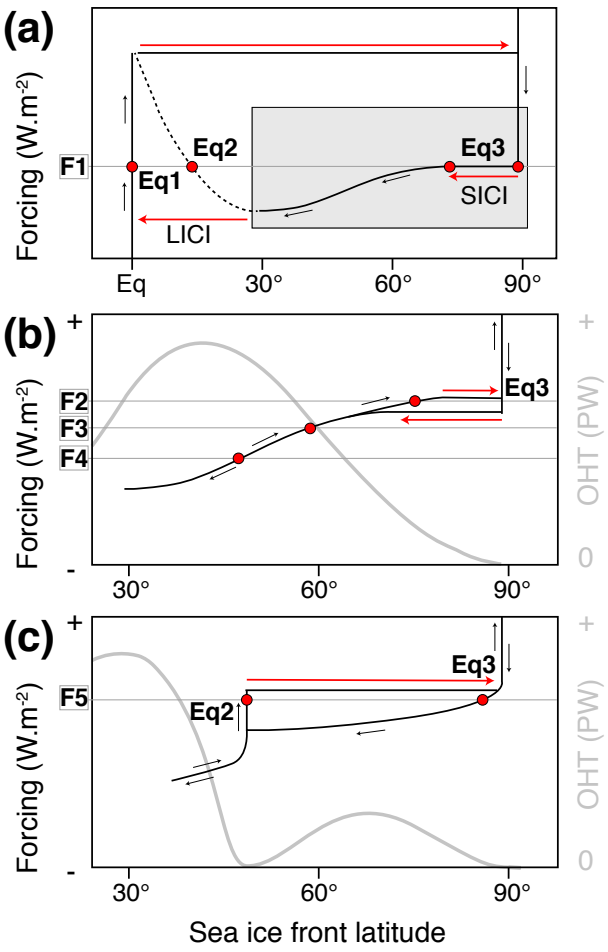

CPD
10, 2767–2804, 2014

Effect of the Ordovician paleogeography on the (in)stability of the climate

A. Pohl et al.

Figure 11. (a) Graph showing the latitude of the sea ice front (x-axis) vs. the climatic forcing (y-axis) for a classical Budyko-Sellers type EBM. Dark arrows indicate the pathway described by the model through a whole cycle of forcing decrease and increase. Red arrows account for major climatic instabilities. Red circles represent the sea ice edge latitudes corresponding to each analytical solution for a given climatic forcing F1. Dashed lines represent regions that are correct analytical solutions but which instability makes unrealizable within the model. *SICI: Small Ice Cap Instability; LICI: Large Ice Cap Instability.* **(b)** Same plot as **(a)** focusing on the domain shaded in grey in **(a)**. The forcing is decreased and then increased without reaching the snowball equilibrium Eq1. Several forcing values (F2, F3 and F4) are represented, each one leading to a single ice cap of finite size (red circles). The OHT pattern corresponding to the purely diffusive transport characteristic of classical EBM is overlayed in grey (right y-axis). **(c)** Same plot as **(b)** for the extended EBM from Rose and Marshall (2009) (see the main text for explanations) in which the OHT pattern is modified (grey curve). Note the two ice caps of finite size corresponding to the forcing level F5. **(a)** is adapted from North et al. (1981), **(b)** and **(c)** are modified after Rose and Marshall (2009).

CPD
10, 2767–2804, 2014

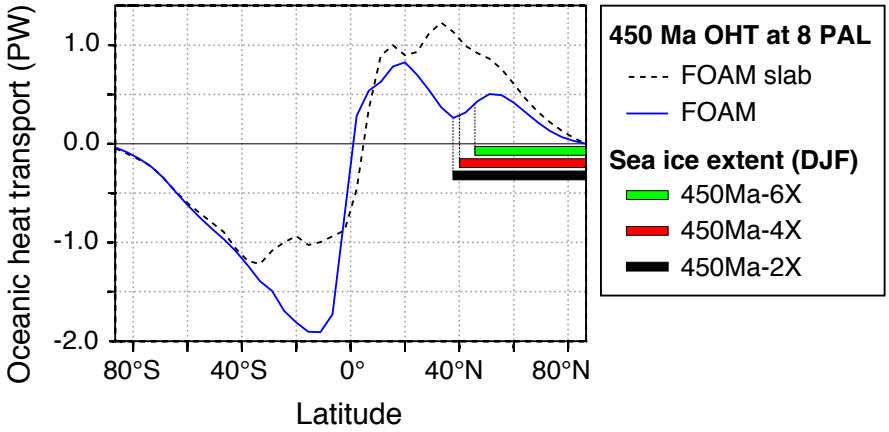

Figure 12. Comparison of the total OHT at 450 Ma and at 8 PAL for the slab-version of FOAM and for the fully coupled ocean–atmosphere-sea ice version of FOAM. The OHT pattern is relatively stable when CO_2 is varied. Color bars represent the maximum (boreal winter) Northern Hemisphere sea ice extension simulated within the cold climatic mode at 450 Ma with the fully coupled model.

CPD
10, 2767–2804, 2014